OXFORD

Cerebral Cortex, 2023, 1–10
https://doi.org/10.1093/cercor/bhad182
Original Article

Metal deposits associated with brain atrophy in the deep gray matter nucleus in Wilson's disease

Zihuan Huang[1,†], Jie Yang[2,†], Dingbang Chen[3], Xiangxue Zhou[3], Xia Xiao[3], Junqiao Wang[1], Mengzhu Wang[4], Jing Zhao[1,*], Jianping Chu[1,*]

[1]Department of Radiology, The First Affiliated Hospital of Sun Yat-Sen University, Guangzhou 510080, Guangdong Province, China,
[2]Institute of Biomedical Engineering, Shenzhen Bay Laboratory, Shenzhen 518000, Guangdong Province, China,
[3]Department of Neurology, The First Affiliated Hospital of Sun Yat-Sen University, Guangzhou 510080, Guangdong Province, China,
[4]Department of MR Scientific Marketing, Siemens Healthineers, Guangzhou 510120, Guangdong Province, China

*Corresponding author: Dr. Jianping Chu, Department of Radiology, The First Affiliated Hospital of Sun Yat-sen University, 58 Zhoushan Road 2nd, Guangzhou, Guangdong, 510080, P.R. China. Email: chujping@mail.sysu.edu.cn or Dr. Jing Zhao, Department of Radiology, The First Affiliated Hospital of Sun Yat-sen University, 58 Zhoushan Road 2nd, Guangzhou, Guangdong, 510080, P.R. China. Email: zhaoj23@mail.sysu.edu.cn

†Zihuan Huang and Jie Yang contributed equally to this work.

Regional atrophy and metal deposition are typical manifestations in Wilson's disease, but their relationship has not been systematically investigated. We aim to investigate the association of regional brain atrophy and metal deposition in the deep gray matter nucleus at MRI in Wilson's disease. We acquired the structural and susceptibility mapping and performed a cross-sectional comparison of volume and susceptibility in deep gray matter nucleus. The most extensive and severe atrophy was detected in brain regions in neuro-Wilson's disease, as well as the most widespread and heaviest metal deposits. Metal deposits were significantly negatively correlated with volume in the bilateral thalamus, caudate, and putamen. None of correlation was found between the clinical score with volume or susceptibility in the focused regions. In the 1-year follow-up analysis, the volume of right thalamus, globus pallidus, and brainstem and the susceptibility of the left caudate have decreased significantly as the symptom improvement. In Wilson's disease, phenotypes have varied scope and extend of volumetric atrophy and metal deposits. This study is expected to take the lead in revealing that in neuro-Wilson's disease, greater regional atrophy associated with heavier metal deposits in Wilson's disease. Moreover, after 1-year treatment, the imaging data have changed as the patient's condition improvement.

Key words: Wilson's disease; atrophy; susceptibility; deep gray matter nucleus; UWDRS.

Introduction

Wilson's disease (WD) is an autosomal recessive disorder caused by mutated ATP7B gene, which encodes the enzyme ATPase 2, a transport protein that eliminates coper from the liver via bile and plasma. The disturbed copper metabolism results in toxic effects on the hepatocytes and increasing copper in the circulation which leads to metal accumulation in the liver, central nervous system, cornea, and other organs (Ala et al. 2007; EASL Clinical Practice Guidelines. 2012; Członkowska et al. 2018). WD has a wide spectrum of clinical presentations: hepatic, neurological, ophthalmic, and psychiatric dysfunction. When copper is primary deposited in the liver, this stage is referred to as the hepatic form of WD (hep-WD). In later stages of the disease, metal accumulating in the central nervous system results in a neurological form of WD (neuro-WD) manifesting in neurologic and psychiatric symptoms (Ferenci et al. 2003).

Recently, MRI serves as an indispensable tool to provide noninvasive evaluation of brain abnormalities in WD. Excess metal can cause toxicity, which brings damage to neurons and astrocytes and activates macrophages, resulting in myelin degeneration, gliosis, and profound neuronal loss (Dusek et al. 2017). The lenticular nuclei, caudate, and thalamus were the most prominent regions to be affected, followed by brainstem (Sinha et al. 2006; Prashanth et al. 2010; Smolinski et al. 2019). A great number of morphometric studies (Stezin et al. 2016; Zou et al. 2019; Dusek et al. 2021; Song et al. 2021) revealed global and local brain atrophy, white matter changes and tissue sponginess in subcortical gray matter (caudate, putamen, globus pallidus, thalamus, amygdala, red nucleus, substantial nigra, brainstem), and cortical structures (left precentral gyrus, left insula, bilateral primary motor, premotor and visual cortices) in WD patients. In phenotype comparison, patients with neurologic presentations had lower gray matter volumes than that patient with hepatic presentations including bilateral caudate, putamen, and nucleus accumbens by morphometric analysis (Shribman et al. 2022; Tinaz et al. 2021; Viveiros et al. 2021). However, our previous morphometric studies (Zou et al. 2019; Song et al. 2021) have not contained the hep-WD subgroup. Given that the extent and severity of atrophy varies in phenotypes, our present cohorts were further enlarged and subdivided into neuro-WD, presenting neurological and psychiatric symptoms, and hep-WD, presenting altered liver function but absent neuropsychiatric manifestations.

We have detected and quantified regional morphometric abnormalities, in term of both volume and shape (Zou et al. 2019; Song et al. 2021). However, metal accumulation in brain structures has not been focused. Higher susceptibility in deep gray matter (DGM) nucleus in WD patients compared with controls has been reported in previous in-vitro studies utilizing quantitative susceptibility mapping (QSM) and R2* relaxometry (Li et al. 2020; Fritzsch et al. 2014; Dusek et al. 2018;

Received: April 1, 2023. **Revised:** May 3, 2023

Dezortova et al. 2020; Saracoglu et al. 2018), suggestive of increased metal deposits and confirmed at autopsy (Litwin et al. 2013; Dusek et al. 2017). Whole-brain QSM (Shribman et al. 2022) detected that neuro-WD had increased susceptibility in the bilateral putamen, cingulate, and medial frontal cortices compared with hep-WD. But what kind of metal deposits causing the aberrant structural brain changes remains unclear (Litwin et al. 2013; Fritzsch et al. 2014; Dusek et al. 2017, 2018; Saracoglu et al. 2018; Dezortova et al. 2020; Li et al. 2020). Given that this disorder is caused by unbalanced copper metabolism, metal overload and its toxic effect built WD pathological and clinical basis. We hypothesize that there are disparate levels of metal accumulation in brain within phenotypes and excess metal deposits could cause the morphometric alternation.

The aim of this study was to quantitatively examine volume and susceptibility in DGM nucleus in WD phenotypes and to explore their relationship. The association between image data with the Unified Wilson's Disease Rating Scale (UWDRS) was also explored. Moreover, we also analyzed the longitudinal metal and morphometric change in the patients after treatment.

Materials and methods

Study participants

The study was approved by the local committee of the First Affiliated Hospital of Sun Yat-Sen University ([2020]056). Only data of patients that provided signed consent to use their clinical and imaging data for research purpose were enrolled.

We included consecutive treatment-naïve adult patients diagnosed with WD in our department, according to Leipzig criteri[4] and confirmed by genetic testing between November 2020 and May 2021. The patient cohort was classified into 2 clinical phenotypes (i.e. predominantly neurological and predominantly hepatic). The presence of cornea copper deposits in either eye (the Kayser-Fleischer ring) was determined by an ophthalmologist in a slip-lamp examination. Exclusion criteria for all participants consisted of a history of neurological or psychiatric diseases (except secondary symptoms induced by WD) or contraindications for MRI. Disease duration was defined as the time from first hepatic or neurological symptoms, which did prompt a diagnostic work-up, to the time of this MR scan. Besides 4 patients are newly diagnosed, the rest have undergone anti-copper treatment since the definite diagnosis for ranging from 0.2 to 39 years.

In this study, we retrospectively analyzed data of 75 patients with WD on chronic anti-copper treatment (41 with neuro-WD: 29 M/12F, median age 26.0 [21.0–32.5] years; 34 with hep-WD: 20 M/14F, median age 24.0 [17.8–26.0] years); and 34 healthy controls (16 M/18F, median age 25.0 [23.0–28.0] years). All participants are right-handed. All subjects underwent 3.0 T and only 33 neuro-WD patients have undergone UWDRS assessment. Higher scores indicate greater impairment (Członkowska et al. 2007). In addition, volume and susceptibility were remeasured in 15 posttreatment patients, with an average of a 12-month interval. Table 1 summarizes the clinical and demographic characteristics of all subjects enrolled in this study.

MRI data acquisition

MRI was performed with a 3.0-T scanner (Prisma; Siemens) with a 64-channel birdcage head coil. The MRI protocol included sagittal structural T1-weighted 3D magnetization-prepared rapid acquisition with gradient echo and the following parameters: repetition time msec/echo time msec/inversion time msec, 2,000/2.32/900; flip angle, 8°; field of view, 256×256 mm^3; slices, 192; voxel resolution, $0.9 \times 0.9 \times 0.9$ mm^3; bandwidth, 200 Hz per pixel; and generalized auto-calibrating parallel acquisition acceleration factor, 2; scan time, 4 min and 6 s. For QSM, an axial multi-echo gradient-recalled echo pulse sequence was included, and the parameters were as follows: repetition time 35 msec; 4 equidistant echo time between 7.50 and 28.26 msec; flip angle, 20°; field of view, 220×220 mm^3; slices, 64; voxel resolution, $0.5 \times 0.5 \times 2$ mm^3; bandwidth, 260 Hz per pixel; scan time, 8 min and 56 s.

Subcortical nucleus volumetric segmentation

For subcortical nucleus volumetric analysis, all data were processed using the FreeSurfer software (version 6.0.0). the preprocessing stream comprise in the FreeSurfer analysis pipeline includes some preliminary steps as follows (Desikan et al. 2006; Fischl et al. 2004): motion correction, affine registration to Talariach atlas, intensity normalization, skull stripping, automatic subcortical segmentation including neck removal, segmentation of WM and GM structures (https://surfer.mnr.mgh.harvard.edu), and so on. After that, the midbrain is cut from the cerebrum in step Cut/Fill. The software was used to segment T1-weighted images into a total of 45 subcortical anatomical ROIs. Estimated subcortical nucleus volume was, respectively, extracted from the aseg.stats, which is part of the results produced from the "recon-all" batch command. It should be noted that no manual correction was made to any of the FreeSurfer results to ensure a valid analysis. However, a visual inspection was conducted to check the quality of the FreeSurfer results. According to our previous studies (Zou et al. 2019; Song et al. 2021), we decide to pick the following subcortical nucleus as ROIs:bilateral thalamus, caudate, putamen, globus pallidus, brainstem, hippocampus, amygdala, and accumbens. To normalize the estimated total intracranial volumes (eTIV), we defined atrophy degree as volume of DGM nuclei/eTIV and compared atrophy degree for detecting subtypes atrophy patterns. Additionally, atrophy rate of the neuro-WD subgroup was also calculated: atrophy rate = |mean volume of patients-mean volume of controls|/mean volume of controls.

QSM and data processing

The morphology-enabled dipole inversion (MEDI) toolbox is a collection of MATLAB routines for reconstructing whole-brain QSM (http://pre.weill.cornell.edu/mri/pages/qsm.html). In short, the pipeline consisted of the following (de Rochefort et al. 2010; Liu et al. 2012): (i) continuous Laplacian-based phase unwrapping, (ii) variable, spherical mean value property-based background field removal using a 10 mm starting kernel radius, and (iii) nonlinear MEDI with $\lambda = 1{,}000$.

The significant altered DGM structures were chosen as the target labels. Then the target labels were extracted from FreeSurfer for brain binary mask individually. After this, the brain binary mask would have the same space coordinates as the whole-brain QSM map, individually. The whole-brain QSM map was set as background image. As regions of interest, including bilateral thalamus, caudate, putamen, and globus pallidus, brain binary masks were automatically drawn to cover their own susceptibility map by MRIcronGL software (http://www.mccauslandcenter.sc.edu/mricrongl/). Subsequently, mean susceptibility values of the target labels were calculated. The flow chart was shown in Fig. 1.

Statistical analysis

Statistical analyses were performed with SPSS (Version 16.0; IBM, Armonk, NY, United States). A possible influence of sex between groups was evaluated using a chi-square test and the influence of age was tested by 1-way ANOVA. The difference of disease duration between phenotypes was analyzed using Mann–Whitney

Table 1. Clinical and demographic characteristics of study participants.

Demographic	neuro-WD ($n = 41$)	hep-WD ($n = 34$)	Controls ($n = 34$)	*P*-value
Gender, Male/female	29/12	20/14	16/18	0.114
Median age [IQR], year	26.0 [21.0–32.5]	24.0 [17.8–26.0]	25.0 [23.0–28.0]	0.050
Median disease duration [IQR], year	8.0 [2.0–14.0]	9.0 [1.4–13.3]		0.848
Treatment mode				
D-PEN	2	0		
Zinc salts	1	7		
Combination of D-PEN and zinc	26	19		
Combination of DMPS and zinc	4	2		
Combination of D-PEN, zinc, and DPMS	9	6		
Median UWDRS score [IQR][a]	21.0 [14.0–33.3]			

Note. Except where indicated, data are numbers of the whole study participants. D-PEN, D-penicillamine; DMPS, sodium dimercaptosulphonate; UWDRS, Unified Wilson's Disease Rating Scale. [a]Data are numbers of neuro-WD enabled to finish the UWDRS assessments ($n = 33$).

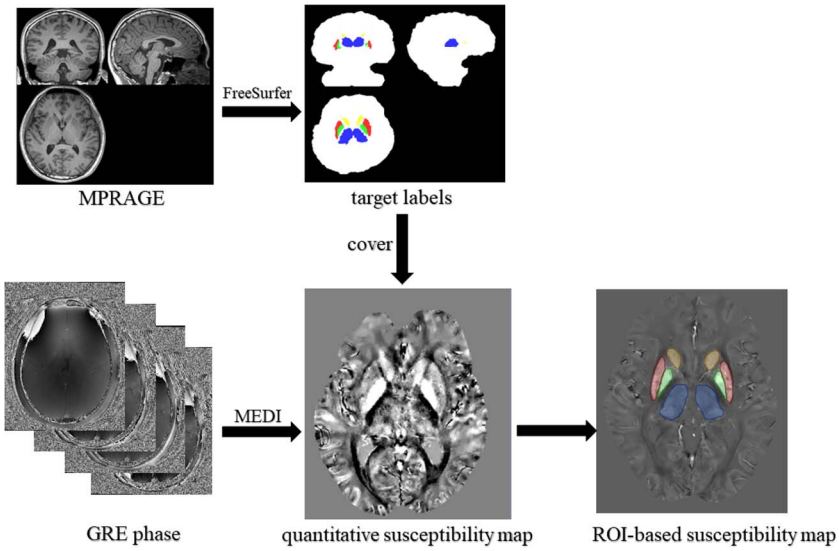

Fig. 1. The flow chart of combining FreeSurfer and MEDI toolbox.

U-test. Normality testing was performed before statistical comparison using the Shapiro–Wilk test. Volumetry and mean susceptibility between groups were tested using Kruskal–Wallis *H*-test. Spearman correlation coefficient analysis was used to assess the correlation between each subcortical nucleus volume with susceptibility value and between imaging data with the total UWDRS score. Longitudinal analysis of multiple measures used the paired samples *t*-test. *P*-value < 0.05 was considered statistical significance.

Results

Participant characteristics

All participants, namely 41 neuro-WD, 34 hep-WD, and 34 healthy controls, were eligible for MRI. There were no significant differences within 3 subgroups with respect to sex ($X^2 = 4.340$, $P = 0.114$) or age ($P = 0.050$). The disease duration in neuro-WD and hep-WD is 8.00 [2.00–14.00] and 9.00 [1.40–13.30], respectively. There is no significant difference of disease duration between phenotypes ($P = 0.848$). The clinical and demographic characteristics for all the subjects are listed in Table 1.

Region of interest-based volumetric pairwise comparison

After being adjusted according to eTIV, the most extensive and severe atrophied DGM was observed in neuro-WD. In neuro-WD, bilateral thalamus, caudate, putamen, globus pallidus, accumbens, and brainstem all atrophied relative to controls; except the right thalamus, the rest nucleus also atrophied relative to hep-WD. Only bilateral thalamus atrophied in hep-WD compared with controls and the most atrophied volume in neuro-WD, followed by hep-WD and the controls exhibited the largest volume. No significant difference of volume was found in bilateral hippocampus and amygdala between subgroups. In neuro-WD, the highest atrophy rate is putamen (left: 49.91%, right: 48.30%). The volume maps of 3 subgroups of sample were exhibited in Fig. 2A. The details are shown in Table 2 and Fig. 2.

Region of interest-based susceptibility pairwise comparison

The most extensive and excess metal deposits was also observed in neuro-WD. In neuro-WD patients, bilateral thalamus, caudate, putamen, and globus pallidus demonstrated higher susceptibility than that in the hep-WD or controls. Bilateral thalamus and globus pallidus showed higher susceptibility in hep-WD relative to controls. The susceptibility exhibited highest in neuro-WD, followed by hep-WD, and the controls had the minimum value. The susceptibility maps of 3 subgroups of sample were exhibited in Fig. 3A. The details are shown in Table 3 and Fig. 3.

Relationship between morphometry and susceptibility

Surprisingly, in 75 patient cohort, we found significant negative correlation between volume and susceptibility in the following

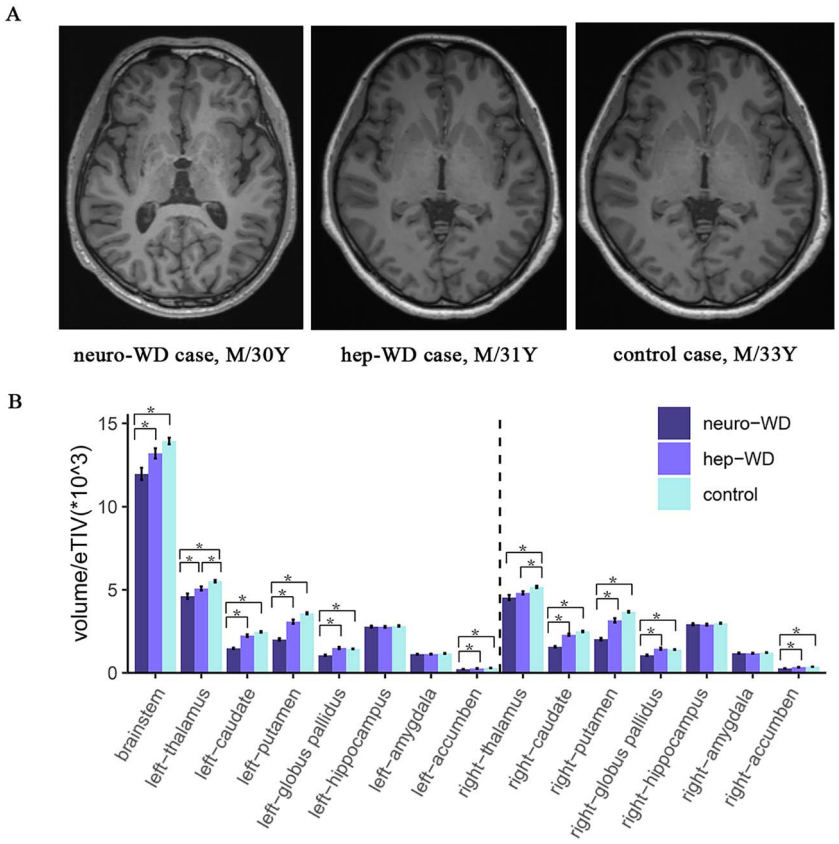

Fig. 2. The volume maps of 3 subgroups of sample were exhibited A). Comparison of atrophy degree in DGM nucleus between subgroups. The volume of brain regions atrophied most severe in the neuro-WD, followed by the hep-WD in the thalamus B). *$P < 0.05$.

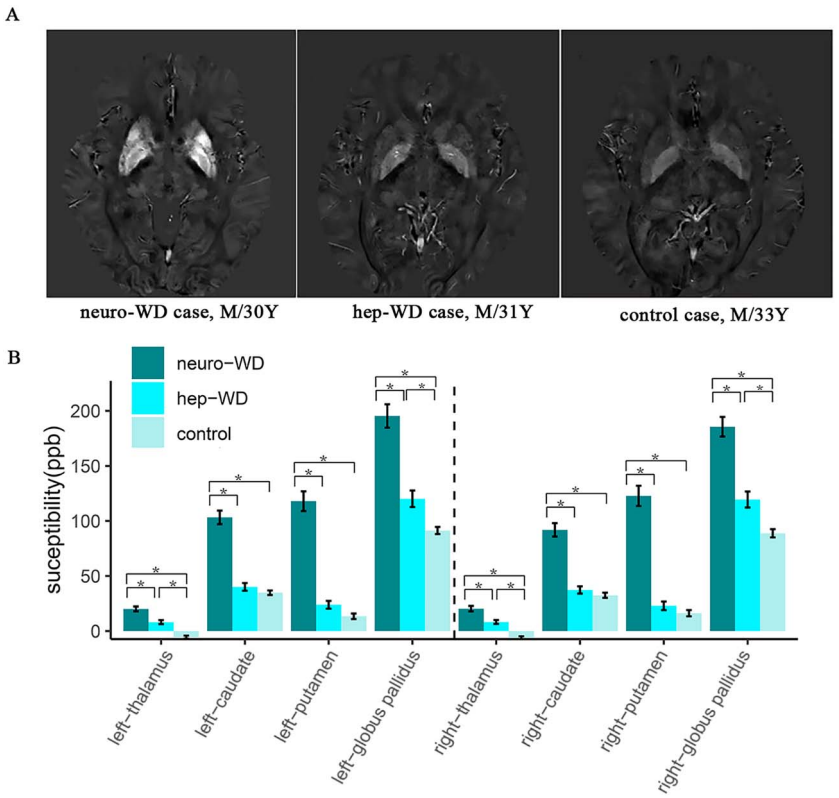

Fig. 3. The susceptibility maps of 3 subgroups of sample were exhibited A). Comparison of susceptibility in DGM nucleus between subgroups. The susceptibility of neuro-WD was the highest, followed by hep-WD, and the controls had the minimal value in the thalamus and globus pallidus B). *$P < 0.05$.

Table 2. Comparison of volume in DGM nucleus of study participants.

		Volume (cm^3)				Volume/eTIV ($^a10^{-3}$)			
Region of interest		neuro-WD	hep-WD	Controls	[a]Atrophy %	neuro-WD	hep-WD	Controls	*P*-value
thalamus	left	6.67 [5.51–7.39]	7.71 [7.03–8.34]	8.38 [7.63–9.09]	20.53%	4.60 [4.05–4.98]	5.20 [4.58–5.50]	5.43 [5.23–5.93]	=0.028, < 0.001, =0.040
	right	6.45 [5.54–7.35]	7.31 [6.75–7.76]	7.88 [7.39–8.25]	18.27%	4.46 [4.09–4.90]	4.93 [4.29–5.13]	5.13 [4.94–5.41]	>0.050, < 0.001, =0.041
caudate	left	2.01 [1.88–2.35]	3.45 [2.93–3.71]	3.83 [3.38–3.98]	47.52%	1.46 [1.32–1.64]	2.15 [1.94–2.62]	2.42 [2.27–2.70]	<0.001, < 0.001, > 0.050
	right	2.18 [2.01–2.53]	3.57 [3.07–3.77]	3.80 [3.53–4.12]	42.63%	1.58 [1.40–1.81]	2.31 [1.96–2.65]	2.47 [2.27–2.70]	<0.001, < 0.001, > 0.050
putamen	left	2.81 [2.36–3.33]	4.86 [3.98–5.34]	5.61 [5.06–5.82]	49.91%	1.92 [1.72–2.25]	3.17 [2.53–3.69]	3.59 [3.31–3.79]	<0.001, < 0.001, > 0.050
	right	2.89 [2.33–3.35]	4.99 [4.03–5.44]	5.59 [5.22–5.60]	48.30%	2.04 [1.69–2.24]	3.29 [2.48–3.75]	3.63 [3.45–3.87]	<0.001, < 0.001, > 0.050
GP	left	1.52 [1.31–1.68]	2.16 [1.94–2.37]	2.14 [2.06–2.34]	28.97%	1.07 [0.89–1.18]	1.47 [1.26–1.62]	1.45 [1.35–1.53]	<0.001, < 0.001, > 0.050
	right	1.50 [1.19–1.78]	1.99 [1.80–2.38]	2.09 [2.01–2.30]	28.23%	1.07 [0.08–1.23]	1.38 [1.16–1.49]	1.40 [1.31–1.47]	<0.001, < 0.001, > 0.050
hippo	left	4.02 [3.74–4.22]	4.14 [3.98–4.49]	4.33 [4.12–4.50]		2.73 [2.55–2.96]	2.84 [2.59–2.95]	2.81 [2.67–3.02]	>0.05
	right	4.17 [3.93–4.49]	4.37 [4.16–4.79]	4.57 [4.28–4.89]		2.88 [2.66–3.10]	2.89 [2.70–3.14]	2.96 [2.84–3.10]	>0.05
amy	left	1.50 [1.19–1.78]	1.99 [1.80–2.38]	2.09 [2.01–2.30]		1.11 [1.02–1.21]	1.13 [1.04–1.24]	1.17 [1.07–1.25]	>0.05
	right	1.71 [1.58–1.84]	1.81 [1.64–1.92]	1.84 [1.69–2.01]		1.14 [1.07–1.29]	1.17 [1.09–1.32]	1.21 [1.14–1.28]	>0.05
acc	left	0.31 [0.25–0.37]	0.40 [0.35–0.51]	0.45 [0.39–0.51]	31.11%	0.21 [0.18–0.26]	0.27 [0.22–0.31]	0.30 [0.26–0.32]	=0.007, < 0.001, > 0.050
	right	0.37 [0.34–0.43]	0.56 [0.44–0.61]	0.55 [0.51–0.60]	32.73%	0.27 [0.23–0.30]	0.35 [0.28–0.40]	0.36 [0.35–0.38]	<0.001, < 0.001, > 0.050
brainstem		16.58 [15.02–18.49]	20.22 [18.90–22.25]	21.01 [20.04–22.67]	21.09%	11.87 [10.75–12.81]	13.39 [12.18–14.79]	13.95 [12.99–14.51]	=0.001, < 0.001, > 0.050

Note: All data were presented as median [IQR]. All the between-group comparisons were tested with Kruskal–Wallis *H*-test. [a]The atrophy rate was calculated in the neuro-WD subgroup. GP = globus pallidus, hippo = hippocampus, amy = amygdala, acc = accumbens.

DGM nucleus, including bilateral thalamus (left, $r = -0.458$, $P = 0.003$; right, $r = -0.398$, $P = 0.010$), caudate (left, $r = -0.560$, $P < 0.001$; right, $r = -0.548$, $P < 0.001$), putamen (left, $r = -0.490$, $P = 0.01$; right, $r = -0.513$, $P = 0.001$). No such correlations were found in the bilateral globus pallidus (left, $P = 0{,}228$; right, $P = 0.236$). Summaries are shown in Fig. 4.

Associations between neuroimaging data and clinical score

Only 33 neuro-WD patients have finished UWDRS assessment. In the region of interest-based volume and susceptibility analysis, none of correlations was found between imaging data with UWDRS total score. The disease duration has negatively correlated with the volume of bilateral putamen (left, $r = -0.356$, $P = 0.023$; right, $r = -0.320$, $P = 0.041$). No significant correlation was found between disease duration and susceptibility in the DGM nucleus.

Volume and susceptibility have changed as the symptom improvement

Repeated clinical assessment and MR scan were available for 15 neuro-WD patients, whose median treatment duration was 1 year. The visible difference was obvious in the conventional images. (One case was shown in Fig. 5A). In the follow-up, these patients have improved in symptoms or remained stable, reflecting the decreased UWDRS scores (Fig. 5B). None of them have aggravated after treatment. Additionally, the volume of right thalamus, global pallidus, and brainstem has decreased in the follow-up analysis. The susceptibility of left caudate has declined after 1-year treatment (details are shown in Table 4 and Fig. 5).

Discussion

We applied quantitative MR methods to determine volumetric and susceptibility alternations in patients with neurological and hepatic forms of WD on long-term anti-copper treatment, aiming at exploring the nature of the residual brain tissue pathology and disease progression. We found extensive and severe atrophy and metal deposits most pronounced in neuro-WD patients. In the focused nucleus, the more severe brain atrophy is associated with the greater metal deposition. After treatment, neuro-WD patients exhibited declined metal deposits in the left caudate with the symptom improvement. The susceptibility is expected to be an imaging biomarker for monitoring therapeutic effect.

We found widespread brain atrophy in DGM nucleus in neuro-WD after adjusting according to individual eTIV, including bilateral thalamus, caudate, putamen, globus pallidus, accumbens, and brainstem, mostly agreeing with our previous study (Zou et al. 2019; Song et al. 2021) and other researches (Stezin et al. 2016; Dusek et al. 2021). Inconsistent with previous studies including ours, they have not detected abnormality in accumbens, but we did find when comparing neuro-WD with controls. Nucleus accumbens, as an important component of the ventral striatum, play important roles in emotion processes, including anxiety-like behaviors and depression (Bewernick et al. 2001; Shirayama and Chaki 2006). This suggests that accumbens atrophy is closely linked with personality and mood disorders.

Besides extensive atrophied lesions, the extent of atrophy varies in both phenotypes. Our previous studies (Zou et al. 2019; Song et al. 2021) have not subcategorized patients and compared their underlying differences. In the present study, the DGM nucleus atrophied greatest in bilateral thalamus in neuro-WD,

Table 3. Comparison of susceptibility in DGM nucleus of study participants.

Region of interest		Susceptibility (ppb)			
		neuro-WD	hep-WD	Controls	*P*-value
thalamus	left	17.60 [9.01–29.59]	9.50 [2.96–13.57]	−4.69 [−10.98 to −0.70]	=0.031, < 0.001, < 0.001
	right	18.19 [9.22–31.89]	7.51 [3.08–13.99]	−6.80 [−11.19 to −0.01]	=0.018, < 0.001, < 0.001
caudate	left	96.40 [74.04–126.22]	40.57 [28.28–49.44]	36.18 [29.08–41.99]	<0.001, < 0.001, 1.000
	right	84.94 [65.26–111.74]	37.17 [26.09–45.60]	34.68 [24.36–40.26]	<0.001, < 0.001, 1.000
putamen	left	113.93 [83.67–155.42]	21.01 [6.77–36.44]	11.37 [2.47–27.83]	<0.001, < 0.001, 0.379
	right	122.80 [81.77–154.31]	21.45 [8.65–34.90]	15.51 [1.49–27.15]	<0.001, < 0.001, 1.000
GP	left	186.13 [139.82–242.48]	119.20 [91.33–138.93]	89.67 [77.21–102.37]	<0.001, < 0.001, 0.031
	right	176.12 [143.70–225.10]	120.44 [91.40–137.09]	91.78 [75.99–104.47]	<0.001, < 0.001, 0.024

Note: All data were presented as median [IQR]. All the between-group comparisons were tested with Kruskal–Wallis *H*-test.

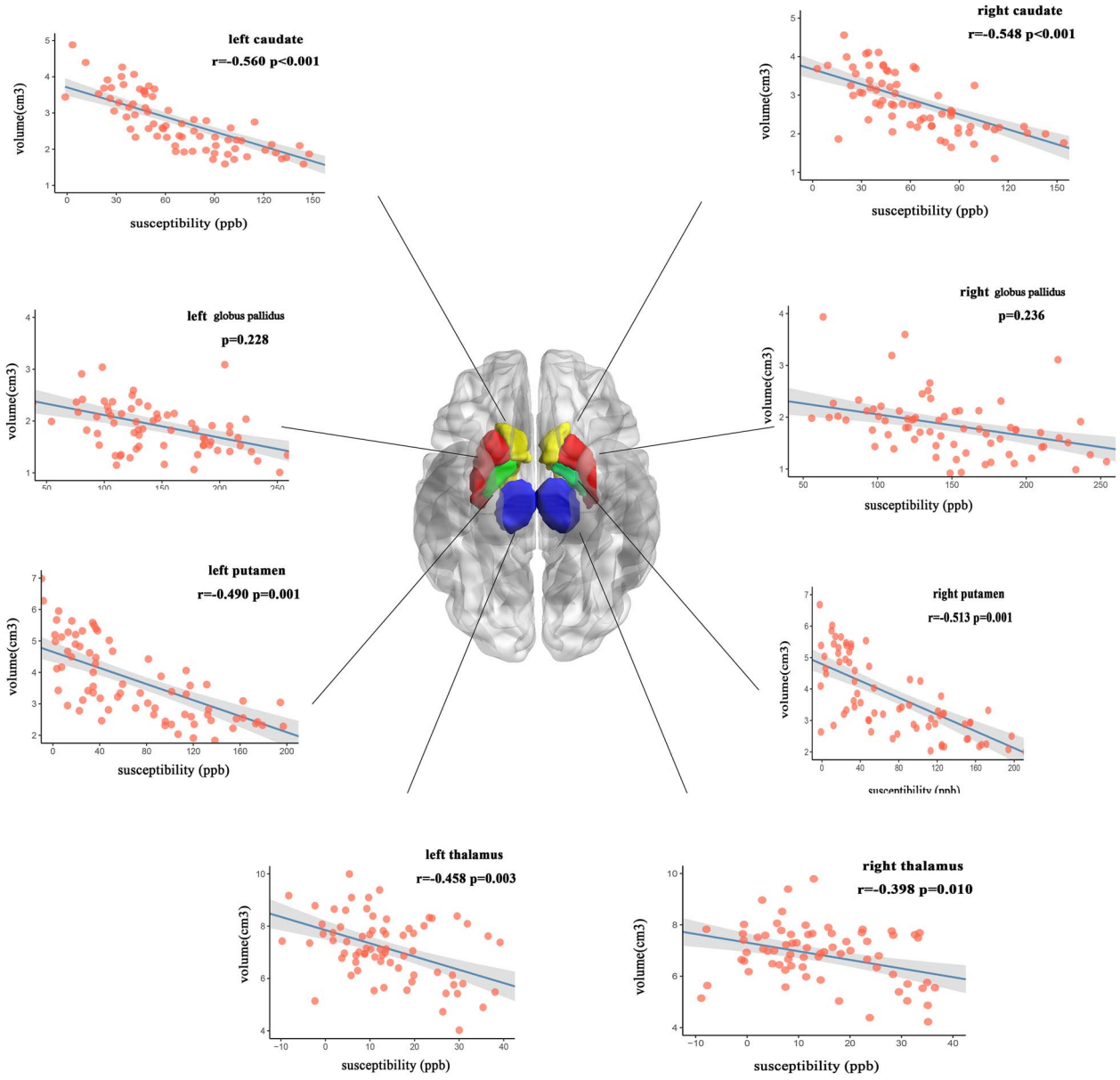

Fig. 4. In 75 patient cohort, we found significant negative correlation between volume and susceptibility in the following DGM nucleus, including bilateral thalamus, caudate, putamen, except bilateral globus pallidus.

followed by hep-WD, and the controls had the largest volume. As expected, the putamen had the greatest atrophy rate, reflecting the most vulnerable region and explaining why the abnormal signal could most frequently have been detected in putamen in WD (Sinha et al. 2006; Smolinski et al. 2019). Additionally, our volumetric analysis demonstrated that bilateral thalamus

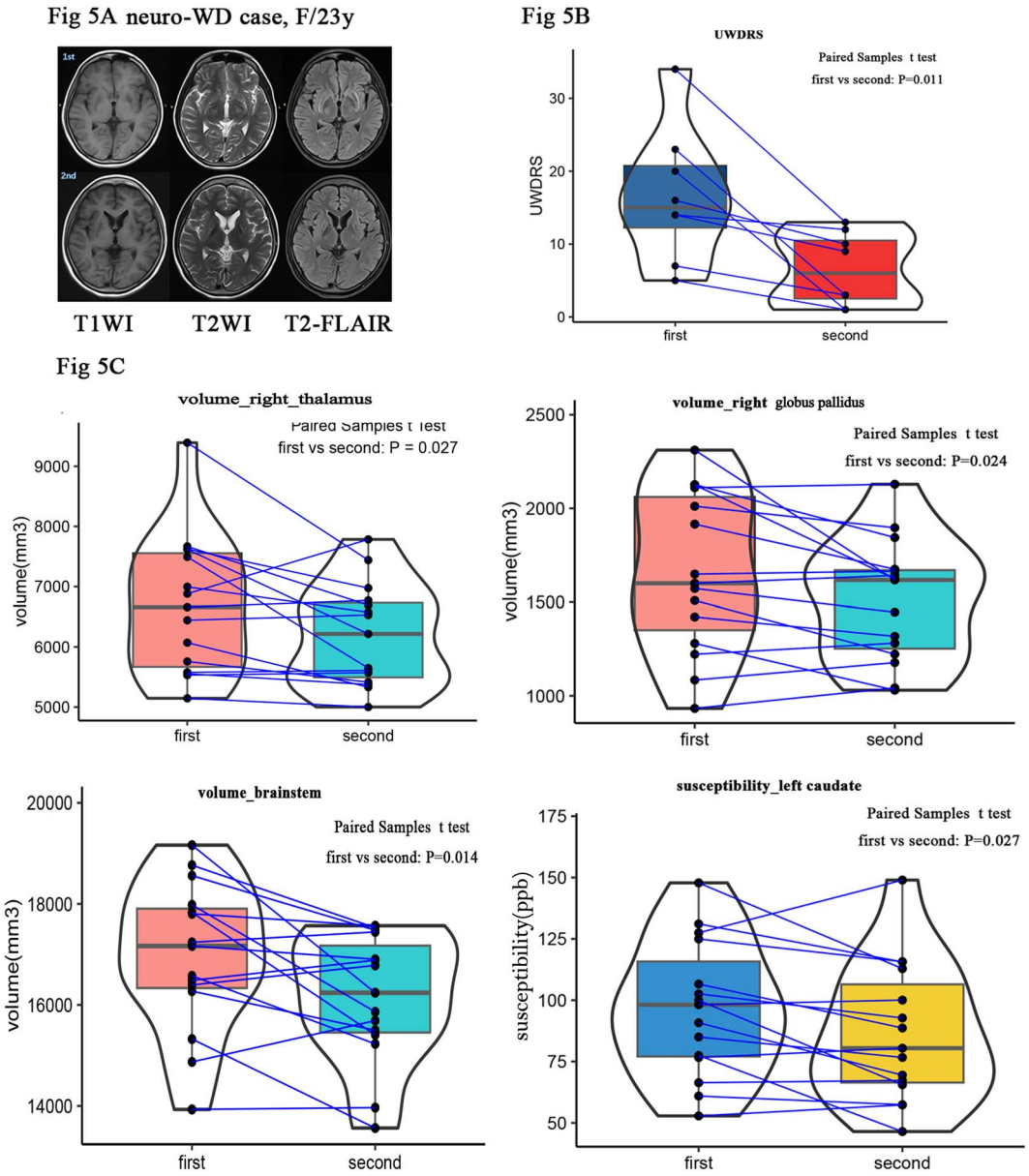

Fig. 5. The case is neuro-WD, F/23, duration: 0.5 years. The visible difference was obvious in the conventional images A). In the 1-year follow-up, the total UWDRS scores have decreased and the patients have improved in symptoms or remained stable B). The volume of right thalamus, globus pallidus, and brainstem has decreased and the susceptibility of left caudate had declined after 1-year anti-copper agent therapy C).

deteriorated further in neuro-WD than that in hep-WD, which partly agreed with the result of VBM-based study reported by Shribman et al. (2022) and Viveiros et al. (2021). We hypothesized that abnormal morphometric findings were mostly initiated in thalamus. This scope and extent of brain atrophy could be compensated in hep-WD patients. As the disease progresses, volumetric atrophy extends diffusely to more brain regions. Further longitudinal studies are needed to prove this inference.

To date, this is the largest sample size of QSM-based study in WD patients. We found neuro-WD had the largest amount of metal deposits in the focused DGM nucleus. Our result of pairwise comparison revealed that bilateral thalamus and global pallidus showed the highest susceptibility in the neuro-WD, followed by hep-WD, and the controls had the minimum value. It is believed that increased magnetic susceptibility in DGM nuclei is likely caused predominantly by an accumulation of paramagnetic metal species, not only copper but also iron (Dusek et al. 2017). The ceruloplasmin, as a ferroxidase enzyme, whose reduction can cause disruptions in iron metabolism. Excess metal causes toxicity, which results in some inflammatory reaction that activated macrophages will swallow the foreigner. Regardless of absent neuropsychiatric symptoms, the elevated metal has deposited in the brain regions in hep-WD patients. Shribman et al. (2022) reported that patients with neurological presentations had higher susceptibility in the bilateral putamen, cingulate, and medial frontal cortices compared with patients with hepatic presentations based on the whole-brain QSM analysis. Fritzsch et al. (2014) found no different susceptibility between neuro-WD with hep-WD, and Dezortova et al. (2020) reported a trend of more metal accumulation in putamen in neuro-WD than that in hep-WD. In early stage, the brain has capability to regulate to compensate the change. If not controlling copper imbalance, the sequential distributed metal metabolism will spread wider, leading to further neuron destruction and eventually clinical disability.

Table 4. The UWDRS and imaging data changes in the 1-year follow-up analysis.

Case	Disease duration (years)	Treatment mode	UWDRS	Volume (cm^3)			Susceptibility (ppb)
			Total score (first/second)	R_thalamus (first/second)	R_pallidus (first/second)	Brainstem (first/second)	L-caudate (first/second)
No.1	2	2	34/13	6.07/5.33	1.65/1.66	16.58/15.23	131.09/115.60
No.2	0.5	1	20/1	5.53/5.57	1.92/1.67	18.77/17.53	106.59/88.68
No.3	9	1	7/3	6.66/6.77	2.01/1.90	16.49/16.88	90.82/69.46
No.4	11	1	14/9	5.76/5.41	1.50/1.64	17.17/16.90	127.48/148.95
No.5	17	1	23/3	5.15/5.00	1.08/1.18	14.87/15.69	98.15/100.05
No.6	0	1	5/1	7.67/6.69	0.93/1.04	16.40/16.78	102.59/92.77
No.7	8	2	14/12	6.44/6.53	2.11/2.13	17.80/17.57	99.94/65.55
No.8	0	2	16/12	5.58/5.61	1.22/1.28	17.24/17.44	60.93/57.42
No.9	35	2	34/10	7.62/6.98	1.28/1.03	17.83/15.41	147.82/112.88
No.10	17	2	NA	5.55/5.38	2.13/1.62	13.93/13.97	77.49/46.47
No.11	21	1	NA	7.00/6.58	2.31/1.62	18.56/17.48	124.96/115.72
No.12	3	1	NA	9.39/7.44	1.57/1.45	19.16/16.24	52.84/57.32
No.13	1	1	NA	6.88/7.78	2.13/1.84	16.27/15.50	85.02/76.67
No.14	10	1	NA	7.49/5.65	1.42/1.32	15.32/13.56	76.63/80.45
No.15	6	2	NA	7.62/6.22	1.51/1.22	17.98/15.86	66.38/67.32

Treatment mode 1: combination of D-penicillamine and zinc salts; 2: sodium dimercaptosulphonate.

The relationship between volumetric alternation and metal accumulation has not been reported so far. This is the first time that reports a significant negative correlation between volume and susceptibility in DGM nucleus, including bilateral thalamus, caudate, and putamen, except the globus pallidus. We believed that metal deposition was the most conspicuous pathogenesis of regional brain atrophy. Heavier metal deposits, greater damage to the neurons. A series of pathological changes initiated by metal toxicity occurred in brain tissue, such as edema, demyelination, necrosis of neuros, which eventually lead to region atrophy and clinical incapacity. But it is noted that the decomposition of necrotic cells could release trace elements, which attract more inflammatory cells to damage the brain. It is a pity that our cross-sectional study could not give the causal relationship.

Paradoxically, the structural alternation initiated in the thalamus whether with volume or susceptibility in hep-WD, but the most atrophied region is the putamen in neuro-WD. It is possible that the scope and extent of volume atrophy and metal accumulation could be compensated by hep-WD patients. When the metabolic incapability extent to putamen or more regions and reached to the irreversible period, it is hard to alleviate the progression even treated with anti-copper agents. This partly suggested that the exacerbation of clinical symptoms was most correlated with the putamen suffering. This has been confirmed in the postmortem study (Dusek et al. 2017), which reported that the most severe pathologic alternation in the putamen and R2* was most strongly correlated with the iron concentration in the putamen.

WD-related morphometric abnormalities were reported in some studies (Stezin et al. 2016; Zou et al. 2019; Dusek et al. 2021; Shribman et al. 2022; Song et al. 2021). Dusek et al. (2021) considered putaminal volume as the only stable factor associated with clinical severity, enabling better prediction of UWDRS than semiquantitative MRI scores (Dusek et al. 2020). Our previous morphometric analysis (Zou et al. 2019) demonstrated that the modified Young Scale negatively correlated with the bilateral putamen and globus pallidus. Another VBM study (Song et al. 2021) reflected that the volume of the right globus pallidus, bilateral putamen was negatively correlated with the Global Assessment Scale score. Li et al. (2020) first demonstrated that susceptibility values were positively correlated with UWDRS score in the caudate, putamen, and red nucleus in WD patients. However, we could not detect any relationship between imaging data with clinical scores in the DGM nucleus. The following reasons are contributed to the disparity: (i) this is the different sample from the former studies: the clinical symptoms of the present study are much slighter and more stable under the effective anti-copper treatment, needless of hospitalization. Contrarily, the neuro-WD patients in the former study presented severe neurologic impairment and psychiatric anomaly, some even deteriorated regardless of intravenous sodium dimercaptosulphonate treatment. (ii) Besides anti-copper agents, some symptomatic treatment would influence the clinical assessment, because of some false improvement. (iii) The study chose the UWDRS total score and has not analyzed the symptom sub-scores.

In our follow-up analysis, the volume of right thalamus, globus pallidus, and brainstem has decreased than before. This is mostly because that cerebral edema has receded after anti-copper therapy, which was shown obviously in the conventional T2WI and T2-FLAIR imaging. Additionally, we did detect that the susceptibility of left caudate has declined after treatment, reflecting the declined cerebral metal deposition. But few structures have changed in susceptibility. Whether susceptibility serve as a valid imaging biomarker for treatment of WD still requires further exploration with larger samples.

In sum, combining QSM with volumetry has a greater evaluation efficacy on brain damage rather than analyze either of them individually. We hypothesized that when a certain amount of metal accumulation but relative slight morphometric alternation was detected, it is a sign of acute toxicity and brain tissue injury stage, which could be controlled by treatment. While extensive and heavy metal accumulation and atrophy have occurred in the DGM nucleus, it is a sign of brain damage deterioration that the disease progresses to an irreversible stage. In this period, the clinical assessment may be associated with volumetry. We hold that the volumetric alternation is a relatively more long-term and irreversible process than metal accumulation. Taken together, combining QSM and morphometry performed well in distinguishing different stages in WD patients, which provide auxiliary information for WD treatment and progression monitoring.

Our study had several limitations. (i) According to prior knowledge, we focused on the most pronounced affected DGM nucleus. A limited number of regions of interest analyzed in QSM prevent evaluating other areas such as substantial nigra, red nucleus, dentate nucleus, and other essential functional cerebral cortex. Therefore, the automatic whole-brain QSM comparison needs further investigation. (ii) The total UWDRS represent the clinical severity, lacking detailed analysis of each item. (iii) This study lacks the follow-up analysis of patients with exacerbation after treatment.

Conclusion

The present study has demonstrated the most extensive and severe volumetric atrophy and heaviest metal deposits in neuro-WD, followed by hep-WD. Metal accumulation was associated with regional brain atrophy, which was suggestive of better performance of combining both neuroimaging data than either one in diagnosing disease stage and predicting process. Moreover, whether volumetry and susceptibility could synchronize with treatment outcome requires further exploration with larger samples, especially the deteriorating cohort even given the therapy.

Acknowledgments

We thank all participants involved in this study and the technical assistance from Siemens Healthineers.

Funding

The National Natural Science Foundation of China (NSFC 82172015); the Natural Science Foundation of Guangdong Province (2021A1515012279) and the Natural Science Foundation of Guangdong Province (2022A1515011264).

Conflict of interest statement: None declared.

Data availability statement

The data that support the findings of this study are available on request from the corresponding author.

References

Ala A, Walker AP, Ashkan K, Dooley JS, Schilsky ML. Wilson's disease. *Lancet*. 2007:369(9559):397–408.

Bewernick BH, Hurlemann R, Matusch A, et al. Nucleus accumbens deep brain stimulation decreases ratings of depression and anxiety in treatment-resistant depression. *Biol Psychiatry*. 2001:67(2): 110–116.

Członkowska A, Tarnacka B, Möller JC, Leinweber B, Bandmann O, Woimant F, Oertel WH. Unified Wilson's Disease Rating Scale - a proposal for the neurological scoring of Wilson's disease patients. *Neurol Neurochir Pol*. 2007:41(1):1–12.

Członkowska A, Litwin T, Dusek P, Ferenci P, Lutsenko S, Medici V, Rybakowski JK, Weiss KH, Schilsky ML. Wilson disease. *Nat Rev Dis Primers*. 2018:4(1):21.

de Rochefort L, Liu T, Kressler B, Liu J, Spincemaille P, Lebon V, Wu J, Wang Y. Quantitative susceptibility map reconstruction from MR phase data using Bayesian regularization: validation and application to brain imaging. *Magn Reson Med*. 2010:63(1): 194–206.

Desikan RS, Ségonne F, Fischl B, Quinn BT, Dickerson BC, Blacker D, Buckner RL, Dale AM, Maguire RP, Hyman BT, et al. An automated labeling system for subdividing the human cerebral cortex on MRI scans into gyral based regions of interest. *NeuroImage*. 2006:31(3):968–980.

Dezortova M, Lescinskij A, Dusek P, Herynek V, Acosta-Cabronero J, Bruha R, Jiru F, Robinson SD, Hajek M. Multiparametric quantitative brain MRI in neurological and hepatic forms of Wilson's disease. *J Magn Reson Imaging*. 2020:51(6):1829–1835.

Dusek P, Bahn E, Litwin T, Jabłonka-Salach K, Łuciuk A, Huelnhagen T, Madai VI, Dieringer MA, Bulska E, Knauth M, et al. Brain iron accumulation in Wilson disease: a post mortem 7 tesla MRI - histopathological study. *Neuropathol Appl Neurobiol*. 2017:43(6): 514–532.

Dusek P, Skoloudik D, Maskova J, Huelnhagen T, Bruha R, Zahorakova D, Niendorf T, Ruzicka E, Schneider SA, Wuerfel J. Brain iron accumulation in Wilson's disease: a longitudinal imaging case study during anticopper treatment using 7.0T MRI and transcranial sonography. *J Magn Reson Imaging*. 2018:47(1): 282–285.

Dusek P, Smolinski L, Redzia-Ogrodnik B, Golebiowski M, Skowronska M, Poujois A, Laurencin C, Jastrzebska-Kurkowska I, Litwin T, Członkowska A. Semiquantitative scale for assessing brain MRI abnormalities in Wilson disease: a validation study. *Mov Disord*. 2020:35(6):994–1001.

Dusek P, Lescinskij A, Ruzicka F, Acosta-Cabronero J, Bruha R, Sieger T, Hajek M, Dezortova M. Associations of brain atrophy and cerebral iron accumulation at MRI with clinical severity in Wilson disease. *Radiology*. 2021:299(3):662–672.

European Association for Study of Liver. EASL clinical practice guidelines: Wilson's disease. *J Hepatol*. 2012:56(3):671–685.

Ferenci P, Caca K, Loudianos G, Mieli-Vergani G, Tanner S, Sternlieb I, Schilsky M, Cox D, Berr F. Diagnosis and phenotypic classification of Wilson disease. *Liver Int*. 2003:23(3):139–142.

Fischl B, van der Kouwe A, Destrieux C, et al. Automatically parcellating the human cerebral cortex. *Cereb Cortex*. 2004:14(1): 11–22.

Fritzsch D, Reiss-Zimmermann M, Trampel R, Turner R, Hoffmann KT, Schäfer A. Seven-tesla magnetic resonance imaging in Wilson disease using quantitative susceptibility mapping for measurement of copper accumulation. *Investig Radiol*. 2014:49(5): 299–306.

Li G, Wu R, Tong R, Bo B, Zhao Y, Gillen KM, Spincemaille P, Ku Y, du Y, Wang Y, et al. Quantitative measurement of metal accumulation in brain of patients with Wilson's disease. *Mov Disord*. 2020:35(10): 1787–1795.

Litwin T, Gromadzka G, Szpak GM, Jabłonka-Salach K, Bulska E, Członkowska A. Brain metal accumulation in Wilson's disease. *J Neurol Sci*. 2013:329(1–2):55–58.

Liu J, Liu T, de Rochefort L, Ledoux J, Khalidov I, Chen W, Tsiouris AJ, Wisnieff C, Spincemaille P, Prince MR, et al. Morphology enabled dipole inversion for quantitative susceptibility mapping using structural consistency between the magnitude image and the susceptibility map. *NeuroImage*. 2012:59(3):2560–2568.

Prashanth LK, Sinha S, Taly AB, Vasudev MK. Do MRI features distinguish Wilson's disease from other early onset extrapyramidal disorders? An analysis of 100 cases. *Mov Disord*. 2010:25(6): 672–678.

Saracoglu S, Gumus K, Doganay S, Koc G, Kacar Bayram A, Arslan D, Gumus H. Brain susceptibility changes in neurologically asymptomatic pediatric patients with Wilson's disease: evaluation with quantitative susceptibility mapping. *Acta Radiol*. 2018:59(11): 1380–1385.

Shirayama Y, Chaki S. Neurochemistry of the nucleus accumbens and its relevance to depression and antidepressant action in rodents. *Curr Neuropharmacol*. 2006:4(4):277–291.

Shribman S, Bocchetta M, Sudre CH, et al. Neuroimaging correlates of brain injury in Wilson's disease: a multimodal, whole-brain MRI study. *Brain*. 2022:145(1):263–275.

Sinha S, Taly AB, Ravishankar S, Prashanth LK, Venugopal KS, Arunodaya GR, Vasudev MK, Swamy HS. Wilson's disease: cranial MRI observations and clinical correlation. *Neuroradiology*. 2006:48(9):613–621.

Smolinski L, Litwin T, Redzia-Ogrodnik B, Dziezyc K, Kurkowska-Jastrzebska I, Czlonkowska A. Brain volume is related to neurological impairment and to copper overload in Wilson's disease. *Neurol Sci*. 2019:40(10):2089–2095.

Song Y, Zou L, Zhao J, Zhou X, Huang Y, Qiu H, Han H, Yang Z, Li X, Tang X, et al. Whole brain volume and cortical thickness abnormalities in Wilson's disease: a clinical correlation study. *Brain Imaging Behav*. 2021:15(4):1778–1787.

Stezin A, George L, Jhunjhunwala K, Lenka A, Saini J, Netravathi M, Yadav R, Pal PK. Exploring cortical atrophy and its clinical and biochemical correlates in Wilson's disease using voxel based morphometry. *Parkinsonism Relat Disord*. 2016:30:52–57.

Tinaz S, Arora J, Nalamada K, Vives-Rodriguez A, Sezgin M, Robakis D, Patel A, Constable RT, Schilsky ML. Structural and functional brain changes in hepatic and neurological Wilson disease. *Brain Imaging Behav*. 2021:15(5):2269–2282.

Viveiros A, Beliveau V, Panzer M, Schaefer B, Glodny B, Henninger B, Tilg H, Zoller H, Scherfler C. Neurodegeneration in hepatic and neurologic Wilson's disease. *Hepatology*. 2021:74(2):1117–1120.

Zou L, Song Y, Zhou X, Chu J, Tang X. Regional morphometric abnormalities and clinical relevance in Wilson's disease. *Mov Disord*. 2019:34(4):545–554.